The Astrophysical Journal Letters, 877:L13 (8pp), 2019 May 20 https://doi.org/10.3847/2041-8213/ab2044

Timing and Origin of the Angrite Parent Body Inferred from Cr Isotopes

Ke Zhu (朱柯)[1], Frédéric Moynier[1,2], Daniel Wielandt[3], Kirsten K. Larsen[3], Jean-Alix Barrat[4], and Martin Bizzarro[3]
[1] Institut de Physique du Globe de Paris, Université de Paris, CNRS, 1 rue Jussieu, Paris F-75005, France; zhu@ipgp.fr
[2] Institut Universitaire de France, 103 boulevard Saint-Michel, Paris F-75005, France
[3] Centre for Star and Planet Formation and Natural History Museum of Denmark, University of Copenhagen, Øster Voldgade 5–7, Copenhagen DK-1350, Denmark
[4] Laboratoire Géosciences Océan (UMR CNRS 6538), Université de Bretagne Occidentale et Institut Universitaire Européen de la Mer, Place Nicolas Copernic, F-29280 Plouzané, France
Received 2019 February 22; revised 2019 May 2; accepted 2019 May 7; published 2019 May 23

Abstract

Angrite meteorites are some of the oldest materials in the solar system. They provide important information on the earliest evolution of the solar system and accretion timescales of protoplanets. Here, we show that the $^{54}Cr/^{52}Cr$ ratio is homogeneously distributed among angrite meteorites within 13 parts per million, indicating that precursor materials must have experienced a global-scale melting such as a magma ocean. The $^{53}Cr/^{52}Cr$ and Mn/Cr ratios are correlated, which is evidence for an initial $^{53}Mn/^{55}Mn$ ratio of $(3.16 \pm 0.11) \times 10^{-6}$. When anchored to the U-corrected Pb–Pb age for the D'Orbigny angrite, this initial $^{53}Mn/^{55}Mn$ corresponds to an absolute age of 4563.2 ± 0.3 Ma, i.e., 4.1 ± 0.3 Ma after Ca–Al-rich inclusion-formation. This age is distinct from that of the volatile depletion events dated by the $^{87}Sr/^{86}Sr$ initial ratio and therefore must correspond to the age of crystallization of the magma ocean and crust formation of the angrite parent body (APB), which can also constrain a slightly bigger size of APB than that of Vesta. Furthermore, this age is similar to those obtained from internal isochrons of the oldest volcanic angrites that cooled rapidly at the surface of the parent body (with ages of 4564 ∼ 4563 Ma), while older than those obtained from plutonic angrites (4561 ∼ 4556 Ma) that cooled down slowly, located deeper within the parent body. This implies that cooling of the APB took at least ∼8 Myr after its differentiation.

Key words: astrochemistry – meteorites, meteors, meteoroids – nuclear reactions, nucleosynthesis, abundances

1. Introduction

Angrites are basaltic meteorites, mainly consisting of Ca–Al–Ti-rich pyroxene, Ca-rich olivine, and anorthitic plagioclase (Keil 2012). Based on U–Pb dating, they crystallized between 4564 and 4556 Ma (Amelin 2008a, 2008b; Connelly et al. 2008). They are divided into plutonic and volcanic origins, with the plutonic, coarse-grained angrites having nearly equilibrated and cooled down slower than volcanic angrites (Keil 2012). Angrites are characterized by the highest Fe/Mn ratio among achondrites (Papike et al. 2003), and a homogeneous oxygen isotopic composition ($\Delta^{17}O = 0.072 \pm 0.007‰$, 1δ) that suggests more likely large-scale melting (magma ocean) on their parent body (Greenwood et al. 2005). Because of their old ages and rapid cooling histories, volcanic angrites (e.g., D'Orbigny, LEW 86010) are traditionally used as time anchors for early solar system chronology (e.g., Lugmair & Shukolyukov 1998; Glavin et al. 2004; Brennecka & Wadhwa 2012; Schiller et al. 2015). They are also the most volatile element depleted and refractory element enriched basalts in the solar system, with ∼1000 times and ∼100 times lower Rb/Sr and K/U ratios, respectively, than CI chondrites (O'Neill & Palme 2008; Day & Moynier 2014). However, the timescales of global-scale melting and volatile depletion of the angrite parent body (APB) remain debated, because it has been suggested that volatile depletion was either nebular (Hans et al. 2013) or after the formation of the parent body (e.g., O'Neill & Palme 2008; Moynier et al. 2012; Pringle et al. 2014; Siebert et al. 2018). Irrespective of the models, the volatile loss must have happened before the crystallization of the magma ocean.

The ^{26}Al–^{26}Mg system ($t_{1/2} = 0.73$ Myr) gives ages for volcanic angrites that are typically ∼5 Ma after formation of solar system when anchored to the canonical initial $^{26}Al/^{27}Al$ ratio (∼5×10^{-5}) (Baker et al. 2005). However, the abundance and homogenous distribution of ^{26}Al in the early solar system are highly debated (Bouvier et al. 2011; Larsen et al. 2011; Schiller et al. 2015; Koefoed et al. 2016). It has been suggested that the inner solar system was depleted in ^{26}Al relative to the abundance in refractory inclusions (Ca–Al-rich inclusions (CAIs) and amoeboid olivine aggregates; Larsen et al. 2011) and that the APB formed with an initial $(^{26}Al/^{27}Al)_0$ ratio of $1.33(+0.21/-0.18) \times 10^5$ (Schiller et al. 2015). Therefore, the relative ages for angrites obtained from the ^{26}Al–^{26}Mg decay system may not be accurate and require further detailed study. The uranium-corrected ^{207}Pb–^{206}Pb dating system, which is free from assumptions of initial homogeneity of the parent nuclide, shows that angrites cooled down between 4564 and 4556 Ma (Amelin 2008a, 2008b; Connelly et al. 2008; Brennecka & Wadhwa 2012; Schiller et al. 2015; Tissot et al. 2017), consistent with the relative ages obtained from the ^{182}Hf–^{182}W (half-life of 8.9 Myr; Markowski et al. 2007; Kleine et al. 2012) and ^{53}Mn–^{53}Cr (half-life of 3.7 Myr; Lugmair & Shukolyukov 1998; Glavin et al. 2004; Shukolyukov & Lugmair 2008; Shukolyukov et al. 2009; Sugiura et al. 2005; Zhu et al. 2019a) decay systems. However, both the U–Pb and ^{182}Hf–^{182}W ages are obtained from internal isochrons, thereby dating the crystallization and cooling of individual angrites. Therefore, they do not reflect the global-scale melting and differentiation event of the APB that would be recorded in

an isochron obtained from bulk samples. While the $^{184}Hf/^{180}W$ ratios do not vary significantly between bulk angrites to provide reliable bulk sample isochrons (Kleine et al. 2012), the Mn/Cr ratio varies from 1 to 10 (Keil 2012), thereby making the determination of a bulk isochron much more feasible. Furthermore, the good agreement between ^{207}Pb–^{206}Pb and ^{53}Mn–^{53}Cr ages of Gujba CB chondrules (Yamashita et al. 2010; Bollard et al. 2015), individual angrites (Sugiura et al. 2005; Kleine et al. 2012), a carbonaceous achondrite (Sanborn et al. 2019), as well as in Allende CV chondrules (Yin et al. 2009a; Connelly et al. 2012) suggests that the initial $^{53}Mn/^{55}Mn$ ratio was homogeneously distributed within the solar system.

The mass-independent Cr isotopic variations, $\varepsilon^{54}Cr$ (per 10,000 deviation of the $^{54}Cr/^{52}Cr$ ratio from the standard NIST SRM 979 representing the Earth Cr isotopic composition), among different clans of meteorites originating in different regions of the solar protoplanetary disk (Trinquier et al. 2007; Qin et al. 2010; Larsen et al. 2011; Warren 2011; Van Kooten et al. 2016), have been proposed to result from the variable distribution of presolar nano-spinels (Dauphas et al. 2010; Qin et al. 2011; Nittler et al. 2018). As such, $\varepsilon^{54}Cr$ variations in meteoritic materials can be used as a proxy for their accretionary regions within the solar system (Olsen et al. 2016; Schmitz et al. 2016; Trinquier et al. 2006; Goodrich et al. 2017; Mougel et al. 2017; Kruijer et al. 2018; Sanborn et al. 2019; Zhu et al. 2019a). In detail, carbonaceous (CC) and ordinary chondrites (OC) show positive ($+0.4 \sim +1.6$) and negative (~ -0.4) $\varepsilon^{54}Cr$ signatures, respectively (Trinquier et al. 2007; Qin et al. 2010; Göpel et al. 2015; Pedersen et al. 2019), while the Earth (0.10 ± 0.12), the Moon (0.09 ± 0.08), and enstatite chondrites (EC, 0.02 ± 0.11) are isotopically identical (Mougel et al. 2018). Moreover, most differentiated planetary bodies are characterized by deficits in $\varepsilon^{54}Cr$, decreasing in the following order: Earth = Moon > Mars (SNCs) > Vesta (HEDs) $\geqslant$ Ureilite parent body (Trinquier et al. 2007; Qin et al. 2010; Yamakawa et al. 2010; Van Kooten et al. 2017; Mougel et al. 2018). However, there are only published $\varepsilon^{54}Cr$ data for three angrites showing variable values of -0.36 ± 0.07 for Angra dos Reis, -0.45 ± 0.05 for NWA 2999, and $\sim 0.00 \pm 0.10$ for D'Orbigny (Glavin et al. 2004; Trinquier et al. 2007; Schiller et al. 2014). These globally ^{54}Cr poor compositions suggest an inner solar system origin, but the range of variation may reflect a lack of homogenization of the APB, which would be at odds with the O isotopic data (Greenwood et al. 2005). On the other hand, it is possible that some of the data may not be accurate. A more systematic Cr isotopic study on a large range of angrites is necessary to solve this potential issue.

Here, we report the first systematic high-precision mass-independent Cr isotopic data for seven angrites (including four volcanic and three plutonic) establishing a bulk ^{53}Mn–^{53}Cr isochron to date the differentiation of APB. Then the nucleosynthetic $\varepsilon^{54}Cr$ can be used to trace the origin of APB and also test the magma ocean model.

2. Samples and Methods

Pieces of three plutonic angrites, NWA 4931, NWA 2999, and NWA 10463 (NWA 4931 and NWA 2999 are paired specimens), and four volcanic angrites, NWA 1296, NWA 7203, D'Orbigny, and Sahara 99555, were crushed to powders using an agate mortar, and 20–40 mg were weighed and transferred into Teflon bombs. Samples were dissolved following the protocol described in Inglis et al. (2018) using Teflon bombs and an Analab EvapoClean. The procedure involved heating in a concentrated HF and HNO_3 mixture (in 2:1 ratio) at 140°C for 2 days, and subsequent dissolution in aqua regia (concentrated HCl and HNO_3 mixture in 3:1 ratio, also at 140°C) for another 2 days to ensure complete digestion of fluorides and refractory phases such as chromite and spinel. Before chemical separation of Cr, ~10% aliquots were preserved for precise determination of the $^{55}Mn/^{52}Cr$ ratio and major element contents by Multiple Collector Inductively Coupled Plasma Mass Spectrometry (MC-ICP-MS) Neptune Plus and Inductively Coupled Plasma Mass Spectrometry (ICP-MS), respectively, at the Institut de Physique du Globe de Paris (IPGP). The external precisions are <2% for the $^{55}Mn/^{52}Cr$ ratios and $5 \sim 10\%$ for major element concentrations, which were acquired from multiple measurements on the USGS standards PCC-1 and DTS-1.

Chromium (Cr) was purified from ~5 mg aliquots based on a procedure involving a three-step chromatographic ion-exchange purification protocol described in Bizzarro et al. (2011) and Larsen et al. (2018) and using Cr pretreatment procedures to promote appropriate Cr-speciation described in detail in Larsen et al. (2016b). In summary, firstly we used an anion chromatographic purification column to efficiently remove Fe from the remaining sample aliquot in 6M HCl, followed by elution of Cr on a cation exchange column in 0.5M HNO_3 (Bizzarro et al. 2011). Prior to sample loading on the cation column, we used a Cr pretreatment procedure involving dissolution in 10M HCl at >120°C to efficiently promote the formation of Cr(III)-Cl species, which have a low affinity for the cation exchanger and thus elutes early (Trinquier et al. 2008b; Larsen et al. 2016b). The third clean-up column involved Cr purification from potential contaminant Fe (and other high-field-strength elements) and Na (as well as potential organics) on a small cation exchange column using 0.5M HNO_3, 1M HF, and 6M HCl (Larsen et al. 2018). Prior to sample loading onto this last column, we used a Cr pretreatment procedure involving exposure to 0.5M HNO_3 + 0.6% H_2O_2 at room temperature for >2 days to promote the formation of Cr^{3+} (Larsen et al. 2016b). The wash part of the third column was passed through the third column again to achieve a high yield that is between 90% and 99%. The blank of <2 ng is negligible compared to the $1 \sim 15\,\mu g$ of Cr processed through the columns. The final Cr solution obtained was fluxed for 1 day in 200 μl concentrated aqua regia and concentrated HNO_3, respectively, to remove residual organics (i.e., from the cation exchange resin).

The Cr isotopic compositions of the samples were determined by Thermal Ionization Mass Spectrometer Thermo Scientific TRITON at the Centre for Star and Planet Formation, Natural History Museum of Denmark, University of Copenhagen. The filament exhaustion sample standard bracketing approach was used, and the detailed methods of measurement and data reduction are described in Van Kooten et al. (2016, 2017). Every sample spread over $2 \sim 4$ turrets, and was run $8 \sim 22$ times. The $^{53}Cr/^{52}Cr$ and $^{54}Cr/^{52}Cr$ ratios were normalized to a $^{50}Cr/^{52}Cr$ ratio of 0.051859 using an exponential law (Lugmair & Shukolyukov 1998), and are

Table 1
Mn–Cr Data of Bulk Angrites

Name	Mass (g)	Type	$^{55}Mn/^{52}Cr$	error	$\varepsilon^{53}Cr$	2SE	$\varepsilon^{54}Cr$	2SE	*N*
NWA 4931	0.0278	Plutonic	0.96	0.02	0.17	0.05	−0.51	0.08	8
NWA 2999	0.0434	Plutonic	0.98	0.02	0.25	0.05	−0.31	0.10	16
combined	⋯	⋯	0.97	0.03	0.21	0.07	−0.41	0.13	
NWA 1296	0.0279	Volcanic	5.25	0.11	1.43	0.04	−0.55	0.11	20
NWA 7203	0.0297	Volcanic	5.57	0.11	1.59	0.05	−0.35	0.18	22
NWA 10463	0.0357	Plutonic	2.33	0.05	0.41	0.06	−0.45	0.11	15
Sahara 99555	0.0300	Volcanic	9.54	0.19	2.51	0.06	−0.43	0.13	16
D'Orbigny	0.0444	Volcanic	7.30	0.15	1.83	0.04	−0.42	0.09	9
Angra dos Reis[a]	⋯	Plutonic	⋯	⋯	⋯	⋯	−0.36	0.07	⋯
NWA 4801[a]	⋯	Plutonic	⋯	⋯	⋯	⋯	−0.35	0.06	⋯
PCC-1	⋯	⋯	⋯	⋯	0.00	0.07	0.06	0.09	9
DTS-1	⋯	⋯	⋯	⋯	0.09	0.03	0.09	0.08	11

Note. NWA 4931 and NWA 2999 (paired) are recognized as one sample with average data, since they are paired meteorites. The error for $^{55}Mn/^{52}Cr$ is regarded as 2%.
[a] The $\varepsilon^{54}Cr$ data for Angra dos Reis and NWA 4801 are from Shukolyukov et al. (2009) and Trinquier et al. (2007).

Table 2
Major Elemental Content Data of Bulk Angrites

Sample Name	Mg	Al	Ca	Ti	V	Cr	Mn	Fe	Ni	Fe/Cr	Mg#
NWA 4931	124909	55815	64650	2666	70	2512	1895	207899	2519	77	58%
NWA 2999	96451	37130	72001	3192	82	2105	1635	231508	5294	102	49%
NWA 1296	43709	75669	113067	5227	134	532	2218	196033	18	342	34%
NWA 7203	44272	77870	121870	5914	126	497	2187	197172	22	369	34%
NWA 10463	49407	58331	117816	7005	153	1078	2002	187470	127	161	38%
Sahara 99555	38804	65052	112737	5596	130	274	2065	196101	54	663	32%
repeat	36538	57154	102275	5373	132	297	2077	193653	46	605	31%
D'Orbigny	35918	75742	109811	4608	121	295	1701	163973	26	517	34%

Note. The elemental concentrations have a (2σ) uncertainty of 5%–10%. Mg# (Mg/Mg+Fe) and Fe/Cr are calculated by atom ratios.

expressed in the epsilon notations:

$$\varepsilon^{x}\mathrm{Cr} = \left(\frac{(^{x}\mathrm{Cr}/^{52}\mathrm{Cr})_{\mathrm{sample}}}{(^{x}\mathrm{Cr}/^{52}\mathrm{Cr})_{\mathrm{NIST\ SRM\ 979}}} - 1 \right) \times 10{,}000 \qquad (1)$$

with $x = 53$ or 54.

The reproducibility of NIST SRM 979 for $\varepsilon^{53}Cr$ and $\varepsilon^{54}Cr$ is 0.02 and 0.04 respectively (2SE, $N = 62$). In order to confirm the accuracy of the data, the Cr isotopic composition of the PCC-1 and DTS-1 reference materials were also measured.

3. Results

The Cr isotopic data as well as the $^{55}Mn/^{52}Cr$ ratios of the seven bulk angrites are reported in Table 1 together with two $\varepsilon^{54}Cr$ data from the literature, NWA 4801 and Angra dos Reis (Trinquier et al. 2007; Shukolyukov et al. 2009). In addition, available $\varepsilon^{54}Cr$ data from the literature for angrites NWA 4801 and Angra dos Reis are also listed (Trinquier et al. 2007; Shukolyukov et al. 2009). The $\varepsilon^{53}Cr$ values of the bulk angrites correlate with their $^{55}Mn/^{52}Cr$ ratios, yielding a slope of 0.279 ± 0.010, corresponding to the $^{53}Mn/^{55}Mn$ ratio of $(3.16 \pm 0.11) \times 10^{-6}$ (2σ) and an initial $\varepsilon^{53}Cr$ of -0.10 ± 0.06 (MSWD = 4.2), calculated by model 1 of IsoplotR (Vermeesch 2018; Figure 2). Volcanic angrites have higher Mn/Cr ratios and $\varepsilon^{53}Cr$ values relative to plutonic angrites. The paired angrites, NWA 2999 and NWA 4931, have similar elemental contents and Cr isotope compositions. All the angrites have similar $\varepsilon^{54}Cr$ values within uncertainty, with an average value of -0.42 ± 0.13 (2SD, $N = 8$). The reference materials PCC-1 and DTS-1 show terrestrial Cr isotopic composition (Trinquier et al. 2007; Qin et al. 2010; Mougel et al. 2018), confirming the data accuracy. The major element contents of the bulk angrites are reported in Table 2, which are consistent with literature data for the same samples within ~10% uncertainty (Jambon et al. 2005; Keil 2012; Riches et al. 2012; Baghdadi et al. 2015).

4. Discussion

4.1. Homogeneous $\varepsilon^{54}Cr$

The $\varepsilon^{54}Cr$ values of all angrites are similar within uncertainty (Table 1), with an average value of -0.42 ± 0.13 (2SD, $N = 8$). In particular, our new value for D'Orbigny ($\varepsilon^{54}Cr = -0.42 \pm 0.09$) is different from that of $\sim 0 \pm 0.10$ by Glavin et al. (2004). Given that the $\varepsilon^{54}Cr$ value reported here for D'Orbigny is consistent with that of the other seven angrites, we speculate that the value reported by Glavin et al. (2004) may not be accurate to the stated uncertainties. It has been hypothesized that the growth of asteroidal bodies such as the APB was assisted by the accretion of chondrules (Johansen et al. 2015; Schiller et al. 2018). In these models, accretion of protoplanets occurs by a combination of chondrule and planetesimal accretion. As both chondrules and asteroidal bodies show variable $\varepsilon^{54}Cr$ values (e.g., Trinquier et al. 2007; Olsen et al. 2016; Van Kooten et al. 2016; Zhu et al. 2019a), it is likely that the precursor material that accreted to form the APB had variable $\varepsilon^{54}Cr$. The homogeneous $\varepsilon^{54}Cr$ reported here for the seven angrites implies that their mantle source must

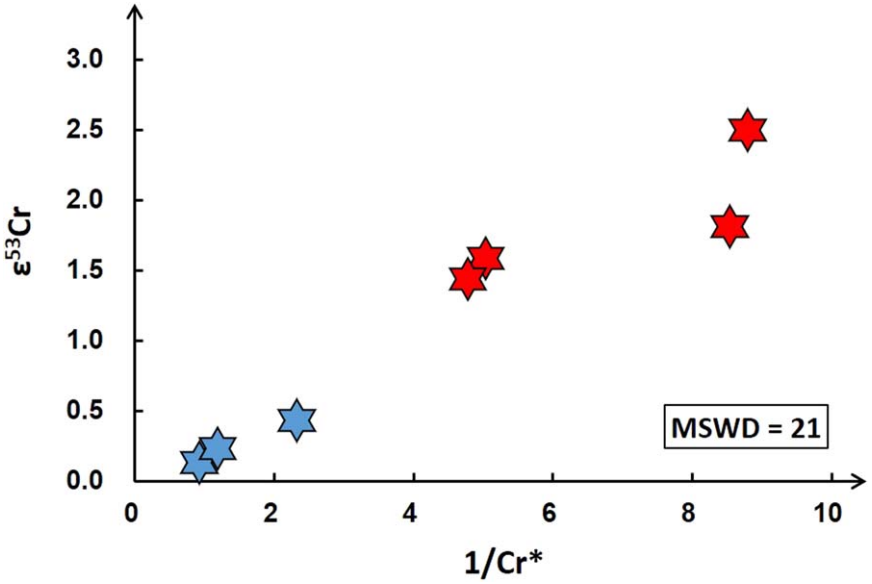

Figure 1. ε^{53}Cr vs. $1/Cr^*$ for angrite samples (the red hexagrams are volcanic angrites, while the blue ones are plutonic angrites). The Cr^* for the samples are their Cr values normalized to the Cr content of NWA 4931. The conservative errors for Cr^* can be estimated as 2%. The larger MSWD (21) suggests that a two-component mixing do not control the ε^{53}Cr variations.

have been well mixed, most likely by a magma ocean, as previously suggested based on O isotopes (Greenwood et al. 2005). Compared to ε^{54}Cr values of other terrestrial planets, we can update the sequence for the variation of ε^{54}Cr values for the inner solar system according to: Earth = Moon > Mars (SNCs) > APB > Vesta (HEDs) ⩾ Ureilite parent body. Furthermore, the homogeneous distribution of ε^{54}Cr among all angrite supports the uses of ε^{53}Cr as a chronological tool without considering possible heterogeneous distribution of Cr isotopes within the APB.

The ε^{54}Cr value can be used to track genetic links between the APB and various chondritic materials. Among chondrites, only ordinary chondrites (OC) possess ε^{54}Cr values that overlap well with those of angrites, with an average of -0.39 ± 0.08 (2SD, $N = 25$; Trinquier et al. 2007; Qin et al. 2010; Pedersen et al. 2019) suggesting similar precursor materials. However, the difference of Δ^{17}O and ε^{50}Ti values for angrites and OCs implies an origin from isotopically distinct precursor materials (Clayton 2003; Greenwood et al. 2005; Trinquier et al. 2009; Warren 2011; Zhang et al. 2012). Such isotopic differences may be explained if the parent body formed by continuous accretion throughout the disk lifetime (Larsen et al. 2016a), recording the continuous influx of CI-like dust from the outer solar system (Schiller et al. 2018). Collectively, the isotopic compositions (ε^{54}Cr, Δ^{17}O, ε^{50}Ti) of angrites suggest that no bulk chondrite materials presently available in our collection represent its undifferentiated precursor material.

4.2. Validity of the ^{53}Mn–^{53}Cr Isochron

Cosmogenic effects can modify the original Cr isotope composition in extraterrestrial samples (Shima & Honda 1966), especially for samples with high Fe/Cr ratio and long exposure ages (i.e., iron meteorites and lunar samples; Qin et al. 2010; Mougel et al. 2018). Since angrites have low Fe/Cr ratios ($70 \sim 600$), short exposure ages ($2 \sim 60$ Ma; Nakashima et al. 2018), and all bulk angrites with various chemical compositions show homogeneous ε^{54}Cr compositions, cosmogenic effects are negligible.

All bulk angrites plot on a single, well-defined correlation line in the ^{53}Mn–^{53}Cr isochron diagram (Figure 2), which could either be interpreted as a mixing line between high-Mn/Cr and low-Mn/Cr ratios components with different ε^{53}Cr or, alternatively, as an isochron. If the correlation were reflecting a mixing process, ε^{53}Cr should correlate with the inverse of the Cr abundance ($1/Cr^*$, defined by the 1/Cr values normalized to the 1/Cr of NWA 4931), which is not the case (Figure 1). In detail, the MSWD = 21 for a plot of ε^{53}Cr versus $1/Cr^*$ is much larger than the MSWD = 4.2 for the correlation line between ^{55}Mn/^{52}Cr and ε^{53}Cr in Figure 2, which is calculated using the model 1 of IsoplotR (Vermeesch 2018). Hence, the Mn–Cr systematics in bulk angrites must define an isochron instead of a mixing line.

4.3. Origin of the Mn/Cr Fractionation

The slope of the isochron records a ^{53}Mn/^{55}Mn ratio of $(3.16 \pm 0.11) \times 10^{-6}$ with an intercept, $(^{53}Cr/^{52}Cr)_0$, of -0.10 ± 0.06. The ^{53}Mn/^{55}Mn ratio corresponds to an absolute age of 4563.2 ± 0.3 Ma (2σ) when anchored to the D'Orbigny angrite, which formed at 4563.37 ± 0.25 Ma (U-corrected ^{207}Pb–^{206}Pb age from Amelin 2008a; Brennecka & Wadhwa 2012) with a ^{53}Mn/^{55}Mn ratio of $(3.24 \pm 0.04) \times 10^{-6}$ (Glavin et al. 2004; Amelin 2008a). The uncertainties on the slope of the isochron, on the half-life of ^{53}Mn, on the U-corrected Pb–Pb age and on the ^{53}Mn/^{55}Mn ratio of the meteorite used as a time anchor are all propagated into the final age uncertainty. This age suggests that the Mn–Cr differentiation for the APB occurred 4.1 ± 0.3 Myr after formation of the solar system (anchored by CAIs, the first solar system solids) (Connelly et al. 2012). Compared to chondrites (including CC, OC and EC), having ^{55}Mn/^{52}Cr ratios ranging from 0.4 to 0.9 (Wasson & Kallemeyn 1988; Qin et al. 2010), bulk angrites have higher Mn/Cr ratios (from 1 to 10). This Mn–Cr elemental fractionation can potentially occur either during (1) core formation (Cr is more siderophile than

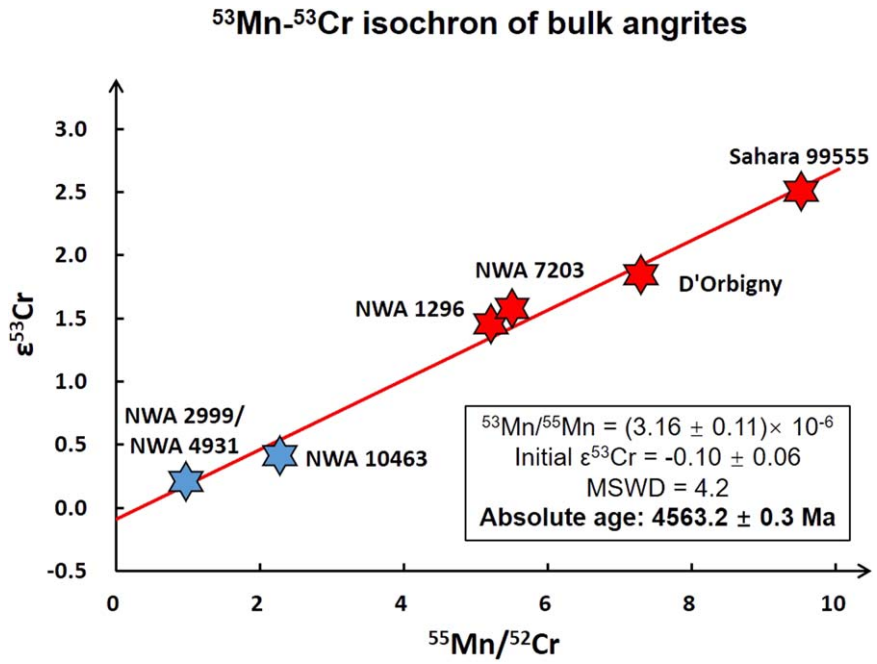

Figure 2. Mn–Cr isochron for bulk angrites. The red hexagrams are volcanic angrites, and blue ones are plutonic angrites. The paired NWA 2999 and NWA 4937 were regarded as one sample. All uncertainties are smaller than the labels, reported as the 2σ. The uncertainty for $^{55}Mn/^{52}Cr$ is 2%. The $\varepsilon^{53}Cr$ values display a strong positive correlation with the $^{55}Mn/^{52}Cr$ ratio. The slope of the line corresponds to 4563.2 ± 0.3 Ma relative to the U-corrected Pb–Pb age for the D'Orbigny angrite.

Mn), (2) evaporation (Cr is more volatile than Mn under oxidizing conditions), and/or (3) mantle/crust differentiation (Cr is more compatible than Mn during igneous fractionation).

The small estimated size of the APB (possibly up to the radius of Vesta (~260 km; Busemann et al. 2006; Scott & Bottke 2011; Russell et al. 2012) implies that the core/mantle equilibrium occurred under low temperature and low pressure, to a maximum of what is expected for Vesta in which only ~2% of Cr could be stored in the core (Zhu et al. 2019b). Since neither Cr nor Mn would partition into the APB's core, metal/silicate fractionation of Cr from Mn cannot create the variable Mn/Cr ratio observed between angrites, and the Mn–Cr age of bulk angrites is not related to the core formation of the APB.

Under relatively oxidizing conditions, relevant to planetary evaporation, Cr becomes more volatile than Mn (Sossi et al. 2016). This would be consistent with the general Mn/Cr excess observed in angrites compared to all chondrite groups and therefore the Mn/Cr ratio could be fractionated during magma ocean degassing. This may also be reflected in the fact that volcanic angrites representing the surface of the APB should experience stronger volatile depletion, with higher Mn/Cr ratio (also higher $\varepsilon^{53}Cr$) relative to plutonic angrites that crystalized deeper in the parent body. Since the ^{87}Rb–^{87}Sr system is a volatile-sensitive chronometer (Rb is much more volatile than Sr; Amelin & Ireland 2013). The age obtained for the Mn/Cr fractionation can be compared to ages obtained from comparing initial $^{87}Sr/^{86}Sr$ ratios (e.g., Gray et al. 1973; Moynier et al. 2012; Hans et al. 2013). However, using the most recent estimate for the CAIs gives Rb/Sr fractionation for the APB within the first 1 Myr of the solar system (Hans et al. 2013), which is inconsistent with the age obtained for the Mn/Cr fractionation (4.1 ± 0.3 Myr) after CAI. This implies that Mn–Cr fractionation was driven by other processes, or at least not only by volatility. However, it should be noted that this approach is limited by the possible estimate of the initial $^{87}Sr/^{86}Sr$ of the CAIs, which is debated (Moynier et al. 2012) and on the uncertainty associated with the $^{87}Rb/^{86}Sr$ ratio of the solar system (~0.90 in carbonaceous chondrites and ~1.2 in the solar photosphere; Gray et al. 1973; Moynier et al. 2012; Hans et al. 2013).

Due to the different geochemical behaviors of Mn and Cr, Mn/Cr fractionation can also occur during magma ocean crystallization and crust formation. During partial melting, Cr is more compatible than Mn, thereby generating higher Mn/Cr ratios in crustal materials than in the residual mantle. This is consistent with higher Mn/Cr ratios in volcanic angrites, compared to those of plutonic angrites, which are slowly cooled cumulate rocks (see Figure 3). Mg# (atom ratio of Mg/(Mg+Fe), an index for magma evolution, anticorrelate well with the Mn/Cr ratio (Figure 4) for all the angrites, which supports the hypothesis that the Mn/Cr fractionation is controlled by magmatic processes.

It is also important to test whether the two groups of samples (plutonic and volcanic angrites) actually define a common isochron or two distinct isochrons, which is also regressed by model 1 of IsoplotR (Vermeesch 2018). When only plutonic angrites are considered, the slope is 0.147 ± 0.068 (MSWD = 1, with the intercept of 0.06 ± 0.13) corresponding to a $^{53}Mn/^{55}Mn$ ratio of (1.67 ± 0.77) × 10^{-6}, which can be translated to 4559.8 ± 2.5 Ma. However, it should be noted that there are only two plutonic angrites and therefore this represents an unreliable two-point isochron. While when it solely includes volcanic angrites, the slope is 0.233 ± 0.019 (MSWD = 2.7, with the intercept of 0.22 ± 0.12) corresponding to a $^{53}Mn/^{55}Mn$ ratio of (3.29 ± 1.36) × 10^{-6}, which can be translated to 4562.3 ± 0.5 Ma. Only the isochron for volcanic angrites is consistent with the bulk angrites isochron in this study [$^{53}Mn/^{55}Mn = (3.16 \pm 0.11) \times 10^{-6}$].

Thermal modeling of the differentiation of the interior planetary shows that a parent body that accreted with a radius >200 km by ~1.5 Myr after CAIs would have a differentiated interior covered by a solid crust (Neumann et al. 2014). The

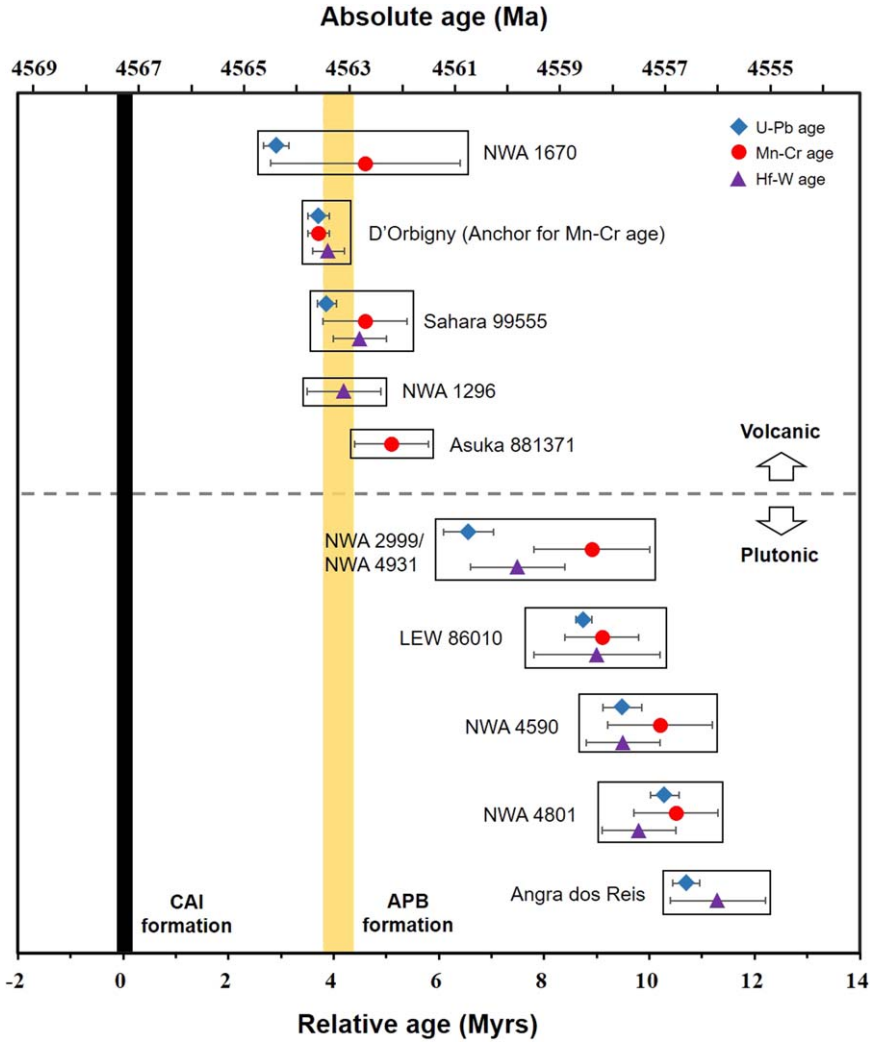

Figure 3. Review for the angrite chronology. The black bar indicates the condensation age for CAI, which represents the zero-point of the solar system (Connelly et al. 2012), while the orange bar is for the age of the angrite parent body, which formed 4.1 Myr after CAI (this study). The internal U–Pb, Mn–Cr, and Hf–W isochron ages for individual angrites are expressed as blue diamonds, red circles, and purple triangles respectively (the age data are from Table 3), and they are consistent with each other, which supports the validity of ^{53}Mn–^{53}Cr and ^{182}Hf–^{182}W dating systems. All the volcanic angrites (upper part) have similar ages with the APB differentiation, which suggests that they should locate in the surface of APB and experience a rapid cooling after the APB differentiation, while all the plutonic angrites are 1 ∼ 8 Ma younger than volcanic angrites. These varied ages between volcanic and plutonic angrites suggest an ∼8 Myr cooling history of APB.

crust of APB formed ∼4 Myr after CAIs, suggesting a parent body with a radius larger than 200 km. This is consistent with Vesta, which has an average radius of 262.7 km and a crust formation age of 4564.8 ± 0.6 Ma (∼2.5 Myr after CAIs, dated by Mn–Cr bulk isochron and anchored to U-corrected D'Orbigny; Trinquier et al. 2008a; Day et al. 2012; Russell et al. 2012). Both Vesta and the APB are rocky bodies, so they should possess similar radiation efficiency during cooling of magma ocean, which is further accompanied by the crust formation. Assuming that ^{26}Al (major radioactive heating source in the early solar system) is distributed homogeneously in the accretion region of Vesta and APB, the delay in the crust formation of the APB relative to Vesta would suggest a larger size for the APB or alternatively that the ^{26}Al were heterogeneously distributed and that the APB were formed from material with a lower ^{26}Al/^{27}Al ratio (Larsen et al. 2011). The paleomagnetic records for angrites indicates that the core dynamo started ∼4 Myr after CAIs (Weiss et al. 2008; Wang et al. 2017), which is identical to the mantle–crust differentiation age inferred here. Thus, the crust formation and core dynamo can occur simultaneously for protoplanets that undergo planetary-scale melting and a global magma ocean.

4.4. Whole Timescale and Cooling History of APB

The ^{53}Mn/^{55}Mn ratio obtained from the bulk angrite isochron (3.16 ± 0.11) × 10^{-6} is similar to that obtained from internal isochrons of individual volcanic angrites (2.85 ∼ 3.24) × 10^{-6} (Glavin et al. 2004; Sugiura et al. 2005). On the other hand, plutonic angrites have systematically lower ^{53}Mn/^{55}Mn (0.96 ∼ 1.28) × 10^{-6} (Lugmair & Shukolyukov 1998; Shukolyukov & Lugmair 2008; Shukolyukov et al. 2009; Yin et al. 2009b), corresponding to an age offset from the bulk isochron of up to 8 Myr (Table 3 and Figure 3). The bulk angrite isochron reflects the original Mn/Cr fractionation event resulting in global melting and differentiation of the APB. Volcanic angrites presumably formed by extrusion of melt from this source reservoir onto the surface of the APB where they cooled down rapidly. Plutonic angrites represent melt pockets in the interior of the planetesimal, which cooled down slowly after the initial differentiation event, and

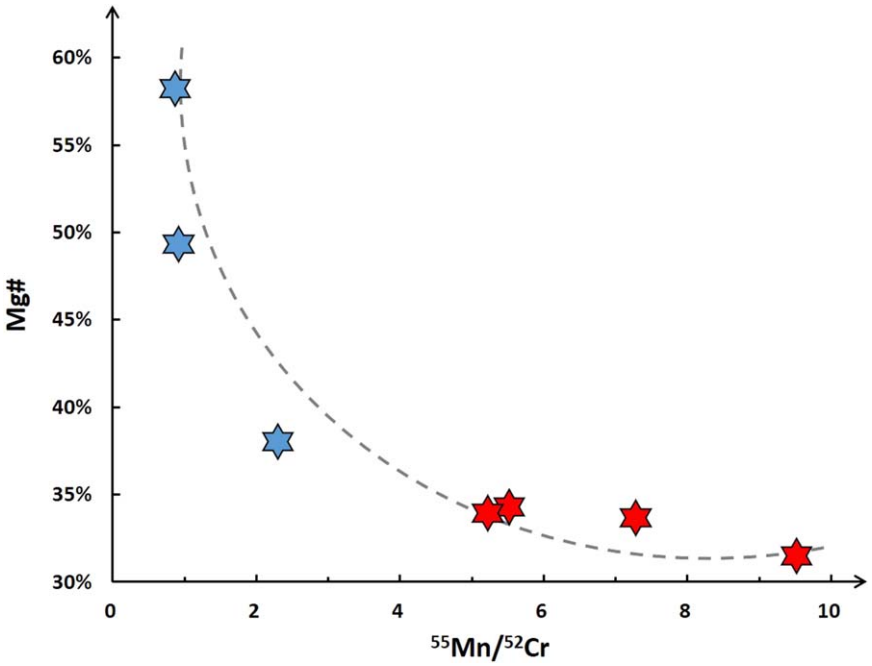

Figure 4. Mg# vs. $^{55}Mn/^{52}Cr$ in bulk angrites. The Mn/Cr ratios of angrites anticorrelates with their Mg#, indicating the magma evolution on APB effectively fractionates the Mn/Cr ratios, so the Mn–Cr age of bulk angrites should record the age of mantle–crust differentiation on the APB.

Table 3
Comparison of Internal Pb–Pb, Mn–Cr, and Hf–W Ages Obtained for Different Angrites

Name	Type	U–Pb	Hf–W	Mn–Cr	$^{53}Mn/^{55}Mn$
NWA 1670	Volcanic	4564.39 ± 0.24	⋯	4562.7 ± 1.8	(2.85 ± 0.92) × 10^{-6}
D'Orbigny	Volcanic	4563.59 ± 0.20	4563.4 ± 0.3	Anchor	(3.24 ± 0.04) × 10^{-6}
Sahara 99555	Volcanic	4563.43 ± 0.18	4562.8 ± 0.5	4562.7 ± 0.8	(2.82 ± 0.37) × 10^{-6}
NWA 1296	Volcanic	⋯	4563.1 ± 0.7	⋯	⋯
Asuka 881371	Volcanic	⋯	⋯	4562.2 ± 0.7	(2.59 ± 0.33) × 10^{-6}
NWA 2999/4931	Plutonic	4560.74 ± 0.47	4559.8 ± 0.9	4558.4 ± 1.1	(1.28 ± 0.23) × 10^{-6}
LEW 86010	Plutonic	4558.55 ± 0.15	4558.3 ± 1.2	4558.2 ± 0.7	(1.25 ± 0.07) × 10^{-6}
NWA 4590	Plutonic	4557.81 ± 0.37	4557.8 ± 0.7	4557.1 ± 1.0	(1.01 ± 0.12) × 10^{-6}
NWA 4801	Plutonic	4557.01 ± 0.27	4557.5 ± 0.7	4556.8 ± 0.8	(1.00 ± 0.07) × 10^{-6}
Angra dos Reis	Plutonic	4556.60 ± 0.26	4556.0 ± 0.9	⋯	⋯

Note. All the Pb–Pb ages are corrected for U isotopic fractionation, Pb–Pb ages are from Amelin & Irving (2007), Amelin (2008a, 2008b), Connelly et al. (2008), Amelin et al. (2011), and Schiller et al. (2015), and U isotope data are from Brennecka & Wadhwa (2012), Connelly et al. (2012), Schiller et al. (2015), and Tissot et al. (2017). For Sahara 99555, its Pb–Pb age is averaged by the 2 data in Amelin (2008b) Connelly et al. (2008), and the NWA 2999 and NWA 4931 are paired meteorites, so their ages are combined. All the Mn–Cr ages are anchored to U-corrected D'Orbigny (Glavin et al. 2004; Amelin 2008a; Brennecka & Wadhwa 2012), the $^{53}Mn/^{55}Mn$ data are from Glavin et al. (2004), Sugiura et al. (2005), Shukolyukov & Lugmair (2008), Shukolyukov et al. (2009), and Yin et al. (2009b). All the Hf–W ages anchored to CAI are from Kleine et al. (2012).

plutonic angrites with varied ages should have been located at different depths within the APB. Therefore, the most likely scenario is that the bulk angrite isochron dates the timing of mantle–crust differentiation of the APB at 4563.2 ± 0.3 Ma. This also gives the latest time at which volatile elements could be lost from the APB. Furthermore, ^{207}Pb–^{206}Pb (U isotope corrected), ^{53}Mn–^{53}Cr (anchored to D'Orbigny), and ^{182}Hf–^{182}W (anchored to CAIs) ages of individual angrites are consistent, supporting the validity for ^{53}Mn–^{53}Cr and ^{182}Hf–^{182}W short-lived dating systems.

In conclusion, global melting caused Cr and O isotopic homogenization of the APB precursors during a magma ocean phase. The magma ocean of the APB cooled at 4563.2 ± 0.3 Ma, which is also the possible time for cease of volatile loss. All the volcanic angrites crystallized quasi simultaneously, 4563 ∼ 4564 Ma, returning similar ages as from the bulk Mn–Cr isochron, suggesting they experienced a very rapid cooling on the surface of the parent body. The plutonic angrites, on the other hand, formed deep within the interior and cooled down slowly until ∼4556 Ma. Therefore, the cooling history of the APB lasted for at least ∼8 Myr.

5. Conclusion

In order to better constrain the formation and evolution of the APB, we measured the Cr mass-independent composition for seven bulk angrites. All the bulk angrites show homogeneous $\varepsilon^{54}Cr$ values, averaging at −0.42 ± 0.13 (2SD, $N = 8$), which supports a global-scale melting event within the APB.

The bulk $^{55}Mn/^{52}Cr$ ratios correlate with $\varepsilon^{53}Cr$, establishing a Mn–Cr fossil isochron, corresponding to an absolute age of 4563.2 ± 0.3 Ma, i.e., 4.1 Myr after CAIs formation. Both volatile processes and mantle–crust differentiation can

potentially cause the variable Mn/Cr ratios observed in volcanic (higher) and plutonic angrites (lower). However, our analysis shows that the age deduced from the bulk isochron records the timing of Mn/Cr fractionation through magmatic processes and mantle–crust differentiation, which can be further used to predict the size of APB (slightly larger than Vesta). The timing of this differentiation event coincides with literature data for the timing of crystallization of volcanic angrites obtained from internal isochrons, suggesting efficient melt-extrusion (high Mn/Cr ratios) onto the surface of the APB within less than 1 Myr after magmatic differentiation. Plutonic angrites represent less fractionated (low Mn/Cr ratios) melt pockets in the planetesimal interior, which cooled down slowly over a much longer time period to crystallize 3–8 Myr after the initial differentiation event.

F.M. acknowledges funding from the European Research Council under the H2020 framework program/ERC grant agreement (#637503-Pristine) and financial support of the UnivEarthS Labex program at Sorbonne Paris Cité (#ANR-10-LABX-0023 and #ANR-11-IDEX-0005-02), and the ANR through a chaire d'excellence Sorbonne Paris Cité. M.B. acknowledges funding from the Danish National Research Foundation (#DNRF97) and the European Research Council (#616027-Stardust2Asteroids). Pierre Burckel was appreciated for elemental analysis on ICP-MS. K.Z. thanks the China Scholarship Council for a PhD fellowship (#201706340161).

ORCID iDs

Ke Zhu (朱柯) https://orcid.org/0000-0003-3613-7239

References

Amelin, Y. 2008a, GeCoA, 72, 221
Amelin, Y. 2008b, GeCoA, 72, 4874
Amelin, Y., & Ireland, T. R. 2013, Eleme, 9, 39
Amelin, Y., & Irving, A. 2007, LPI, 1374, 20
Amelin, Y., Kaltenbach, A., & Stirling, C. 2011, LPSC, 4590, 1682
Baghdadi, B., Jambon, A., & Barrat, J.-A. 2015, GeCoA, 168, 1
Baker, J., Bizzarro, M., Wittig, N., Connelly, J., & Haack, H. 2005, Natur, 436, 1127
Bizzarro, M., Paton, C., Larsen, K., et al. 2011, Journal of Analytical Atomic Spectrometry, 26, 565
Bollard, J., Connelly, J. N., & Bizzarro, M. 2015, M&PS, 50, 1197
Bouvier, A., Spivak-Birndorf, L. J., Brennecka, G. A., & Wadhwa, M. 2011, GeCoA, 75, 5310
Brennecka, G. A., & Wadhwa, M. 2012, PNAS, 109, 9299
Busemann, H., Lorenzetti, S., & Eugster, O. 2006, GeCoA, 70, 5403
Clayton, R. N. 2003, in Solar System History from Isotopic Signatures of Volatile Elements: Volume Resulting from an ISSI Workshop, ed. R. Kallenbach et al. (Dordrecht: Springer Netherlands), 19
Connelly, J. N., Bizzarro, M., Krot, A. N., et al. 2012, Sci, 338, 651
Connelly, J. N., Bizzarro, M., Thrane, K., & Baker, J. A. 2008, GeCoA, 72, 4813
Dauphas, N., Remusat, L., Chen, J., et al. 2010, ApJ, 720, 1577
Day, J. M. D., & Moynier, F. 2014, RSPTA, 372, 20130259
Day, J. M. D., Walker, R. J., Qin, L., & Rumble, D., III 2012, NatGe, 5, 614
Glavin, D., Kubny, A., Jagoutz, E., & Lugmair, G. 2004, M&PS, 39, 693
Goodrich, C. A., Kita, N. T., Yin, Q., et al. 2017, GeCoA, 203, 381
Göpel, C., Birck, J.-L., Galy, A., Barrat, J.-A., & Zanda, B. 2015, GeCoA, 156, 1
Gray, C., Papanastassiou, D., & Wasserburg, G. 1973, Icar, 20, 213
Greenwood, R. C., Franchi, I. A., Jambon, A., & Buchanan, P. C. 2005, Natur, 435, 916
Hans, U., Kleine, T., & Bourdon, B. 2013, E&PSL, 374, 204
Inglis, E. C., Creech, J. B., Deng, Z., & Moynier, F. 2018, ChGeo, 493, 544
Jambon, A., Barrat, J.-A., Boudouma, O., et al. 2005, M&PS, 40, 361
Johansen, A., Mac Low, M.-M., Lacerda, P., & Bizzarro, M. 2015, SciA, 1, 1500109
Keil, K. 2012, ChEG, 72, 191
Kleine, T., Hans, U., Irving, A. J., & Bourdon, B. 2012, GeCoA, 84, 186
Koefoed, P., Amelin, Y., Yin, Q.-Z., et al. 2016, GeCoA, 183, 31
Kruijer, T. S., Borg, L. E., Sio, C. K., & Wimpenny, J. 2018, LPI, 2083, 2517
Larsen, K. K., Schiller, M., & Bizzarro, M. 2016a, GeCoA, 176, 295
Larsen, K. K., Trinquier, A., Paton, C., et al. 2011, ApJL, 735, L37
Larsen, K. K., Wielandt, D., & Bizzarro, M. 2018, Journal of Analytical Atomic Spectrometry, 33, 613
Larsen, K. K., Wielandt, D., Schiller, M., & Bizzarro, M. 2016b, Journal of Chromatography A, 1443, 162
Lugmair, G., & Shukolyukov, A. 1998, GeCoA, 62, 2863
Markowski, A., Quitté, G., Kleine, T., et al. 2007, E&PSL, 262, 214
Mougel, B., Moynier, F., & Göpel, C. 2018, E&PSL, 481, 1
Mougel, B., Moynier, F., Göpel, C., & Koeberl, C. 2017, E&PSL, 460, 105
Moynier, F., Day, J. M., Okui, W., et al. 2012, ApJ, 758, 45
Nakashima, D., Nagao, K., & Irving, A. J. 2018, M&PS, 53, 952
Neumann, W., Breuer, D., & Spohn, T. 2014, E&PSL, 395, 267
Nittler, L. R., Alexander, C. M. D., Liu, N., & Wang, J. 2018, ApJL, 856, L24
Olsen, M. B., Wielandt, D., Schiller, M., Van Kooten, E. M. M. E., & Bizzarro, M. 2016, GeCoA, 191, 118
O'Neill, H. S. C., & Palme, H. 2008, RSPTA, 366, 4205
Papike, J., Karner, J., & Shearer, C. 2003, AmMin, 88, 469
Pedersen, S. G., Schiller, M., Connelly, J. N., & Bizzarro, M. 2019, M&PS, 54, 1215
Pringle, E. A., Moynier, F., Savage, P. S., Badro, J., & Barrat, J.-A. 2014, PNAS, 111, 17029
Qin, L., Alexander, C. M. O. D., Carlson, R. W., Horan, M. F., & Yokoyama, T. 2010, GeCoA, 74, 1122
Qin, L., Nittler, L. R., Alexander, C. M. O. D., et al. 2011, GeCoA, 75, 629
Riches, A. J., Day, J. M., Walker, R. J., et al. 2012, E&PSL, 353, 208
Russell, C., Raymond, C. A., Coradini, A., et al. 2012, Sci, 336, 684
Sanborn, M. E., Wimpenny, J., Williams, C. D., et al. 2019, GeCoA, 245, 577
Schiller, M., Bizzarro, M., & Fernandes, V. A. 2018, Natur, 555, 507
Schiller, M., Connelly, J. N., Glad, A. C., Mikouchi, T., & Bizzarro, M. 2015, E&PSL, 420, 45
Schiller, M., Van Kooten, E., Holst, J. C., Olsen, M. B., & Bizzarro, M. 2014, Journal of Analytical Atomic Spectrometry, 29, 1406
Schmitz, B., Yin, Q.-Z., Sanborn, M., et al. 2016, NatCo, 7, 11851
Scott, E. R., & Bottke, W. F. 2011, M&PS, 46, 1878
Shima, M., & Honda, M. 1966, E&PSL, 1, 65
Shukolyukov, A., & Lugmair, G. 2008, LPI, 1391, 2094
Shukolyukov, A., Lugmair, G., & Irving, A. 2009, LPI, 40, 1381
Siebert, J., Sossi, P. A., Blanchard, I., et al. 2018, E&PSL, 485, 130
Sossi, P., Klemme, S., St.C. O'Neill, H., & Moynier, F. 2016, in Fifteenth International Symposium on Experimental Mineralogy, Petrology and Geochemistry (EMPG-XV) https://www.empg.ethz.ch/
Sugiura, N., Miyazaki, A., & Yanai, K. 2005, EP&S, 57, e13
Tissot, F. L. H., Dauphas, N., & Grove, T. L. 2017, GeCoA, 213, 593
Trinquier, A., Birck, J.-L., & Allégre, C. J. 2006, E&PSL, 241, 780
Trinquier, A., Birck, J.-L., & Allégre, C. J. 2007, ApJ, 655, 1179
Trinquier, A., Birck, J.-L., & Allégre, C. J. 2008a, Journal of Analytical Atomic Spectrometry, 23, 1565
Trinquier, A., Birck, J. L., Allégre, C. J., Göpel, C., & Ulfbeck, D. 2008b, GeCoA, 72, 5146
Trinquier, A., Elliott, T., Ulfbeck, D., et al. 2009, Sci, 324, 374
Van Kooten, E. M. M. E., Schiller, M., & Bizzarro, M. 2017, GeCoA, 208, 1
Van Kooten, E. M. M. E., Wielandt, D., Schiller, M., et al. 2016, PNAS, 113, 2011
Vermeesch, P. 2018, Geoscience Frontiers, 9, 1479
Wang, H., Weiss, B. P., Bai, X., et al. 2017, Sci, 355, 623
Warren, P. H. 2011, E&PSL, 311, 93
Wasson, J. T., & Kallemeyn, G. W. 1988, RSPTA, 325, 535
Weiss, B. P., Berdahl, J. S., Elkins-Tanton, L., et al. 2008, Sci, 322, 713
Yamakawa, A., Yamashita, K., Makishima, A., & Nakamura, E. 2010, ApJ, 720, 150
Yamashita, K., Maruyama, S., Yamakawa, A., & Nakamura, E. 2010, ApJ, 723, 20
Yin, Q.-Z., Amelin, Y., & Jacobsen, B. 2009b, LPI, 40, 2060
Yin, Q.-Z., Yamashita, K., Yamakawa, A., et al. 2009a, LPI, 40, 2006
Zhang, J., Dauphas, N., Davis, A. M., Leya, I., & Fedkin, A. 2012, NatGe, 5, 251
Zhu, K., Liu, J., Moynier, F., et al. 2019a, ApJ, 873, 82
Zhu, K., Sossi, P. A., Siebert, J., & Moynier, F. 2019b, GeCoA, in press